Contrib Mineral Petrol (1991) 107:27–40

Contributions to Mineralogy and Petrology

High pressure experimental calibration of the olivine-orthopyroxene-spinel oxygen geobarometer: implications for the oxidation state of the upper mantle

C. Ballhaus, R.F. Berry, and D.H. Green

Geology Department, University of Tasmania, Hobart, Tas. 7001, Australia

Received April 24, 1990 / Accepted August 16, 1990

Abstract. Synthetic spinel harzburgite and lherzolite assemblages were equilibrated between 1040 and 1300° C and 0.3 to 2.7 GPa, under controlled oxygen fugacity (f_{O_2}). f_{O_2} was buffered with conventional and open double-capsule techniques, using the Fe–FeO, WC–WO_2–C, Ni–NiO, and Fe_3O_4–Fe_2O_3 buffers, and graphite, olivine, and PdAg alloys as sample containers. Experiments were carried out in a piston-cylinder apparatus under fluid-excess conditions. Within the P–T–X range of the experiments, the redox ratio $Fe^{3+}/\sum Fe$ in spinel is a linear function of f_{O_2} (0.02 at IW, 0.1 at WCO, 0.25 at NNO, and 0.75 at MH). It is independent of temperature at given $\Delta \log(f_{O_2})$, but decreases slightly with increasing Cr content in spinel. The $Fe^{3+}/\sum Fe$ ratio falls with increasing pressure at given $\Delta \log(f_{O_2})$, consistent with a pressure correction based on partial molar volume data. At a specific temperature, degree of melting and bulk composition, the Cr/(Cr+Al) ratio of a spinel rises with increasing f_{O_2}. A linear least-squares fit to the experimental data gives the semi-empirical oxygen barometer in terms of divergence from the fayalite-magnetite-quartz (FMQ) buffer:

$$\Delta \log(f_{O_2})^{FMQ} = 0.27 + 2505/T - 400\,P/T - 6\log(X^{olv}_{Fe})$$
$$-3200(1-X^{olv}_{Fe})^2/T + 2\log(X^{sp}_{Fe^{2+}})$$
$$+4\log(X^{sp}_{Fe^{3+}}) + 2630(X^{sp}_{Al})^2/T.$$

The oxygen barometer is applicable to the entire spectrum of spinel compositions occurring in mantle rocks and mantle-derived melts, and gives reasonable results to temperatures as low as 800° C.

Introduction

Oxygen fugacity (f_{O_2}) is a fundamental but little known intensive variable in mantle processes. It influences the P/T position of a mantle solidus and the composition of mantle-derived melts and fluids, and constrains mantle-core equilibria and a number of geophysical properties of the mantle (Arculus 1985; Haggerty 1986; Green et al. 1987; Taylor and Green 1987).

An important source of information on oxidation states is the ferric/ferrous iron ratio in mantle spinels and ilmenites. Provided the thermodynamic parameters are known and activity/composition relations can be assessed, f_{O_2} may be calculated from heterogeneous redox equilibria such as $6\,Fe_2SiO_4$ (olv) + O_2 (fluid) = $3\,Fe_2Si_2O_6$ (opx) + $2\,Fe_3O_4$ (sp) (the fayalite-ferrosilite-magnetite or FFM buffer; Mattioli and Wood 1988), or an analogous reaction involving hematite solid solution in ilmenite (Eggler 1983). In practice, however, f_{O_2} calculations from these equilibria are hampered by uncertainties in the activity/composition relations of magnetite component in spinel. Since magnetite solid solution is low in mantle spinels, typical analytical errors translate into considerable f_{O_2} uncertainties. In addition, spinels become highly ordered below about 800° C and size differences among the trivalent cations require considerable corrections for nonideal mixing.

We have synthesized spinel lherzolite assemblages under $P-T-f_{O_2}$ conditions representative of the Earth's upper mantle. Since the experimental compositions and conditions cover the range in spinel solid solution and possible oxidation states in the mantle, problems with the activity/composition relations of magnetite in spinel do not arise. We formulate a semi-empirical oxygen barometer by adopting regular ionic solution models for olivine and spinel, and an ideal two-site mixing model for orthopyroxene, and then fitting the interaction parameters with our experimental data. The model is applicable to a variety of mantle-derived rocks and spinel-bearing primitive melts.

Experimental technique

Full details of starting mix preparation and experimental techniques are given by Green and Ringwood (1967) and Jaques and Green (1980). Starting compositions used in this study are two fertile MORB pyrolite mixes (Falloon and Green 1987) with bulk

Offprint requests to: C. Ballhaus

Table 1. Starting compositions

	MPY30[a]	MPY55[a]	S1297[b]
SiO_2	35.10	39.07	37.58
TiO_2	0.17	0.07	–
Al_2O_3	18.45	7.58	4.10
Cr_2O_3	6.63	8.06	16.08
Fe_2O_3	0.37	2.12	1.68
FeO	7.21	8.05	8.36
MgO	26.84	30.51	32.20
CaO	5.16	4.44	–
Na_2O	0.21	0.10	–
Cr/(Cr+Al)	0.19	0.42	0.73
Normative compositions (wt%)			
Olivine	18	30	25
Orthopyroxene	24	30	50
Clinopyroxene	21	15	–
Spinel	29	20	25
Melt	8	5	–
H_2O saturated solidi at 1 GPa/NNO (in °C)	~970	~970	~1040

[a] MPY30 and MPY55 are modified MORB pyrolites (Falloon and Green 1987), [b] S1297 is a refractory model harzburgite

Cr/(Cr + Al) ratios of 0.19 and 0.42, and a refractory model harzburgite with a Cr/(Cr+Al) ratio of 0.73 (Table 1), all prepared from spectroscopically pure oxides. The starting compositions are enriched in pyroxene, spinel, and melt components relative to MORB pyrolite or natural harzburgite, to promote multiple phase saturation and large spinel grains at moderate degrees of melting.

All experiments were performed in a 0.5 in. piston-cylinder apparatus. Run conditions were 1040 to 1300° C and 0.3 to 2.7 GPa, with NaCl, NaCl-pyrex, talc, and talc-pyrex assemblies as pressure media. Temperatures were recorded with $Pt/Pt_{90}Rh_{10}$ thermocouples and controlled automatically to within ±4° C of the nominal temperature. A pressure correction of −10% of the nominal load pressure was applied to runs in talc sleeves. All experiments reported are fluid-saturated and well above the H_2O-saturated solidi. Typical run products are shown in Fig. 1.

Buffering of f_{O_2} was achieved with the double-capsule technique (Huebner 1971), using both welded and open inner sample capsules. The oxygen buffers are iron-wüstite (IW), $WC-WO_2$-graphite (WCO), Ni−NiO (NNO), and $Fe_3O_4-Fe_2O_3$ (MH), and f_{O_2}-equations are summarized in Table 2. Nominal f_{O_2} values are corrected to run pressure by a standard pressure correction based on molar volume data. All f_{O_2} values reported here are normalized to the FMQ buffer and quoted as $\Delta \log(f_{O_2})^{FMQ}$.

One of the most important prerequisites for successful oxygen buffering is that the capsule material is inert to both buffer substance and sample material, and that iron loss to the sample container is avoided. The conventional double-capsule technique where the sample is sealed in an inner precious metal capsule meets this requirement only at very high f_{O_2} where iron loss is minimal (Grove 1981). We have used inner metal capsules only in combination with the MH buffer. The sample plus 5 wt% H_2O is welded shut in an inner $Pd_{50}Ag_{50}$ or $Pd_{25}Ag_{75}$ capsule which is placed in a magnetite-hematite (1:9) mechanical mixture containing about 2 wt% H_2O, and then sealed in an outer $Pd_{50}Ag_{50}$ or Pt capsule. Buffering is achieved by hydrogen exchange between buffer and sample through the inner semi-permeable capsule walls, and equilibrium is reached usually after about 24 hours in the presence of hydrous melt. Most MH-buffered runs were carried out for >60 hours, and even at these long run times iron loss to the PdAg sample container proved to be negligible. Magnetite/hematite ratios

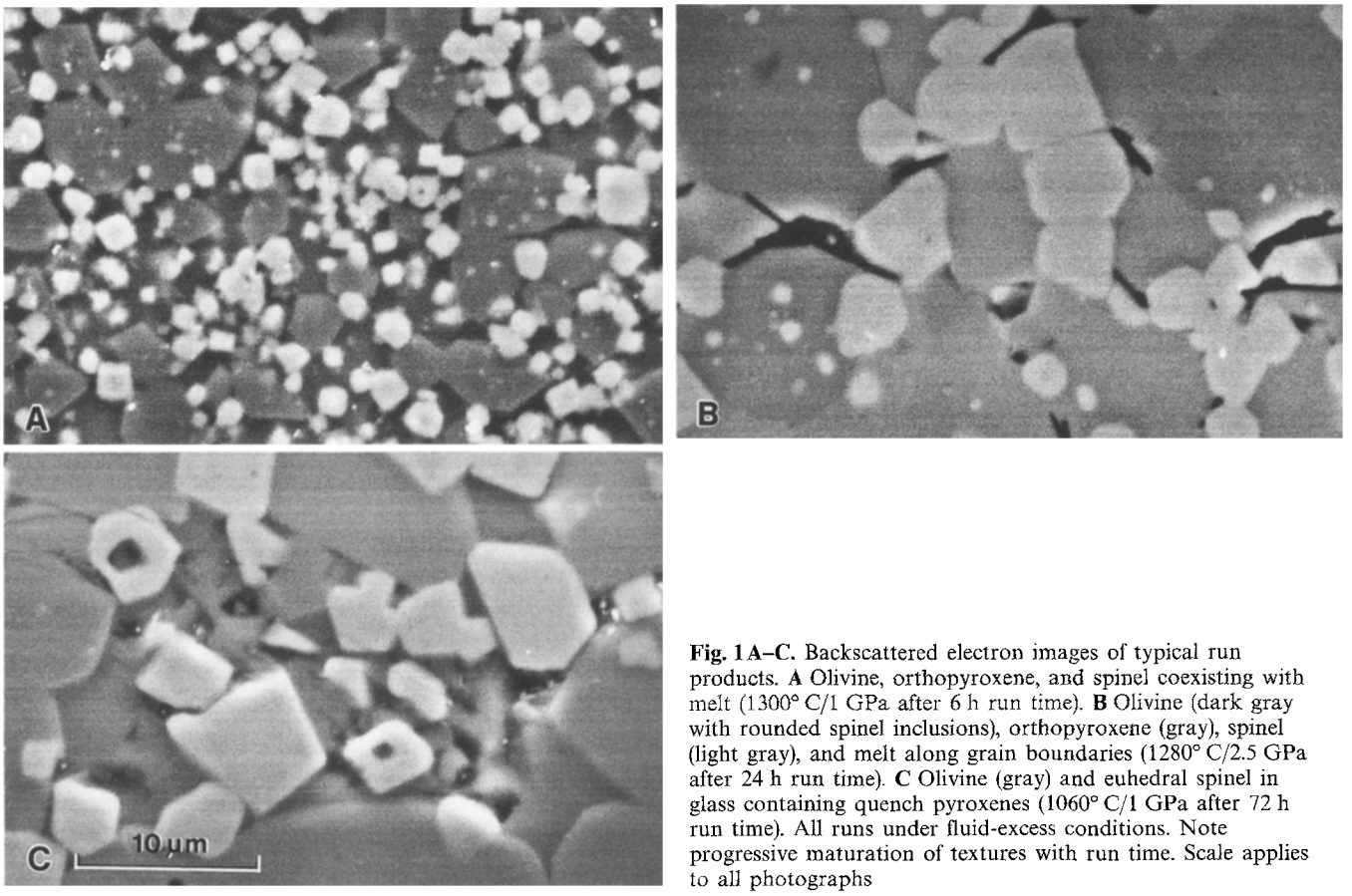

Fig. 1A–C. Backscattered electron images of typical run products. **A** Olivine, orthopyroxene, and spinel coexisting with melt (1300° C/1 GPa after 6 h run time). **B** Olivine (dark gray with rounded spinel inclusions), orthopyroxene (gray), spinel (light gray), and melt along grain boundaries (1280° C/2.5 GPa after 24 h run time). **C** Olivine (gray) and euhedral spinel in glass containing quench pyroxenes (1060° C/1 GPa after 72 h run time). All runs under fluid-excess conditions. Note progressive maturation of textures with run time. Scale applies to all photographs

Table 2. Oxygen buffers used in this study

Buffer	Equation (f_{O_2} in $\log_{10}$ units)	Reference
IW	$14.07-28784/T-2.04\log T+530P/T+0.03P$	(O'Neill 1987a)
WCO	$14.33-29105/T-1.56\log T+660P/T$	(Taylor and Foley 1989)
FMQ	$82.75+0.00484T-30681/T-24.45\log T+940P/T-0.02P$	(O'Neill 1987a)
NNO	$12.78-25073/T-1.1\log T+450P/T+0.025P$	(O'Neill 1987b)
MH	$14.26-24949/T+200P/T-0.05P$	(Schwab and Küstner 1981)

T in Kelvin, P in GPa; pressure corrections from standard molar volume and thermal expansion data

progressively increased to about 1:1 after run times of 3 days, but buffer exhaustion was never observed.

Experiments with the WCO buffer used the technique described by Taylor and Foley (1989). The sample is contained in a graphite container surrounded by the buffer substance, and then sealed in an outer $Pd_{50}Ag_{50}$ or Pt capsule. The buffer material is a mechanical $W-WO_3-C$ (29:1:70) mixture, which reacts in-situ to give WO_2, WC, and graphite. The equilibrium fluid is H_2O-CH_4 (Taylor and Green 1987) and is generated by in-situ combustion of 4 to 6 mg stearic acid added to the buffer. Redox equilibrium is achieved by direct fluid exchange between buffer and sample within about 8–12 h.

Experiments with the IW buffer were carried out in inner capsules of pure iron, which are enclosed in a welded outer Pt capsule. To speed up attainment of chemical equilibrium, the sample was spiked with about 5% metallic iron. The equilibrium fluid at IW conditions is predominantly CH_4-H_2O, which is generated by thermal decomposition of about 5 mg stearic acid added to the sample.

Oxygen buffering is traditionally most difficult in the intermediate f_{O_2} region around FMQ, where graphite is no longer stable but the $Fe^{3+}/\sum Fe$ ratios are too low to permit the use of metal capsules without risking iron loss. Experiments with the NNO buffer have therefore been carried out in sample crucibles made of San Carlos olivine (Fo_{90}). The sample material (6 to 10 mg) is contained in small (1.6 by 1 mm) olivine cylinders with a central bore, covered by an olivine lid, surrounded by a thin lining of olivine powder, packed firmly in the buffer substance (Ni:NiO in the ratio 1:5), and then welded in an outer Pt capsule. The fluid (around 1 µl) is pure H_2O and added to the sample or buffer by microsyringe. Olivine capsules have several advantages in this f_{O_2} range. Redox equilibrium is achieved more rapidly than with the conventional double-capsule technique, i.e. within 3–6 h above 1100° C and about 8 h at 1040° C, because the fluid equilibrates directly with both buffer and sample. Iron loss problems are eliminated as sample and capsule material are in equilibrium. Run times are only limited by the buffering capacity of the buffer substance, which is a function of the difference in the characteristic f_{H_2} of the buffer and f_{H_2} imposed by the graphite furnace. Chemical reaction between the buffer, the olivine capsule, and the fluid phase are negligible. Sample contamination was never encountered because of exceedingly low Ni-solubility in H_2O-rich fluids. Disadvantages of olivine capsules are, however, that the total amount of water partitioning into the sample, and thus the degree of melting and a_{SiO_2}, are more difficult to control than in welded metal capsules.

Analytical techniques

All phases were analysed with a Cameca SX50 electron probe microanalyser calibrated with natural mineral standards (PAP data reduction). Analytical conditions are 15 kV accelerating voltage and 20 nA beam current, using a PET crystal for Ca and Ti, LiF for Cr and Fe, and TAP for the elements Si, Al, and Mg. Counting times varied between 10 and 30 s on both peak and background, depending on concentration levels and count rates for individual crystals.

Calculation of ferric iron in spinel

Ferric iron in spinel was calculated from electron microprobe analyses assuming perfect stoichiometry. To minimize potential systematic errors inherent in this method, the calibration was monitored against an international chromite standard (USNM 117075; Jarosewich et al. 1980) and two synthetic spinels with different Cr/(Cr + Al) ratios synthesized in equilibrium with metallic iron at 1200 and 1250° C at 0.4 GPa. It is reasonable to assume that spinels in equilibrium with metallic iron will be virtually Fe^{3+} free. The calculated $Fe^{3+}/\sum Fe$ ratio of these spinels is 0.02 ± 0.02. Assuming an analytical precision of ± 1 wt% relative for most oxides, we believe that the accuracy and precision with which we can calculate ferric iron in spinel is about 0.02 cations per four oxygens.

Recently, doubts have been raised as to whether ferric iron calculated from electron microprobe analyses will be accurate. McGuire et al. (1989), Wood and Virgo (1989), Dyar et al. (1989), and Canil et al. (1990) have checked stoichiometric $Fe^{3+}/\sum Fe$ ratios in spinel with Mössbauer spectroscopy, and concluded that probe analyses are not accurate enough for reliable Fe^{3+} calculation. We have re-evaluated the original Fe^{3+} data in these papers and consider that their reservations are unfounded (see also Lucas et al. 1988; Mattioli et al. 1989). Expressed in terms of calculated $\Delta \log(f_{O_2})$ the differences between stoichiometric ferric iron and Fe^{3+} as analysed with Mössbauer in all these studies are less than 0.4 log units, and the differences are random (Fig. 2). Only two analyses fall outside the error margin we consider acceptable for a reasonable microprobe analysis. For the particular case of spinel compositions, the result hardly justifies the conclusion that "... calculated Fe^{3+} values based solely on stoichiometry and electron microprobe measurements are inconsistent and generally inaccurate" (Dyar et al. 1989).

Wood and Virgo (1989) suggest that stoichiometric Fe^{3+} values can be improved by checking the calibration against a secondary Fe^{3+} spinel standard previously analysed with Mössbauer spectroscopy. We believe that this method is likely to introduce additional errors. (1) Mössbauer spectroscopy requires relatively large sample sizes of around 200 mg for typical mantle spinels with 10 wt% total iron, and single grains, later selected as secondary standards, need not be representative of the bulk $Fe^{3+}/\sum Fe$ ratio. (2) The interpretation of Mössbauer spectra for spinel is disputed and the errors are potentially large (Dyar et al. 1989); a proper peak assignment requires detailed knowledge of site occupancies of divalent and trivalent iron that is fragmentary at best for intermediate Cr–Al spinels. (3) If an electron microprobe calibration is continuously checked against

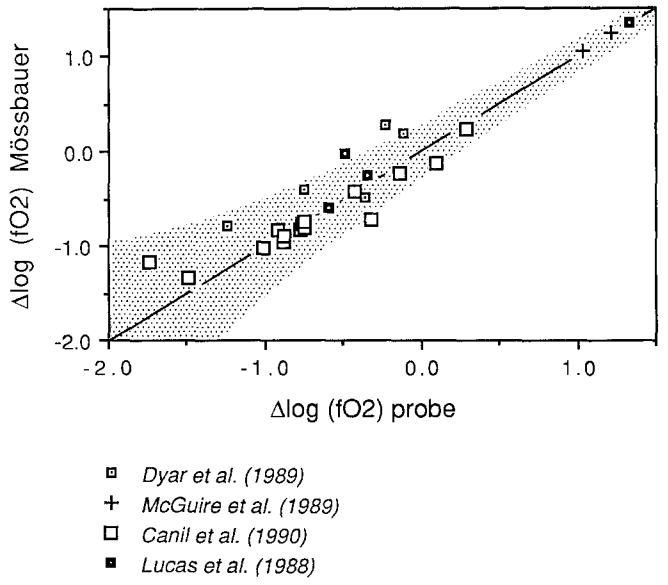

Fig. 2. $\Delta \log(f_{O_2})$ calculated from stoichiometric ferric iron compared with $\Delta \log(f_{O_2})$ based on Mössbauer Fe^{3+}. The stippled field about the 1:1 "best-fit" line illustrates typical uncertainties in calculated $\Delta \log(f_{O_2})$ that are due to analytical errors of $\pm 1.5\%$ relative, assuming that the errors have a cumulative effect on stoichiometric Fe^{3+} (i.e. -1.5 wt% RO, $+1.5$ wt% R_2O_3 and vice versa)

a well-defined spinel standard with a composition close to that of the sample – a standard that is *not* included in the calibration – we have difficulties envisaging how a probe analysis could be corrected to fit the Mössbauer result unless there is reason to suspect nonstoichiometry in spinel.

Attainment of equilibrium

Since all experiments reported here are synthesis experiments, it is important to assess whether equilibrium compositions were produced. Oxide mixes are known to be more reactive than natural minerals and often produce metastable phase assemblages and phase compositions. Equilibrium can only be demonstrated if mineral mixes are used as starting materials and if equilibrium is approached from compositionally opposite directions. For complex $Cr-Al-Fe^{3+}$ spinels however, this requires a multidimensional approach if all exchange vectors are to be reversed.

To test whether equilibrium was reached we have re-ground and then re-equilibrated previously synthesized lherzolite assemblages under the same or different P/T and f_{O_2} conditions and degrees of melting. The results of such "reversals" suggest that $Cr-Al$ and $Mg-Fe^{2+}$ equilibrium within spinel and between spinel and silicates are easily reached with synthesis experiments provided a melt is present; in fact, the reversals under different P/T condition gave slightly larger compositional ranges than the synthesis runs. The redox ratio of a given spinel proved to be difficult to reverse, and two attempts are described below.

The starting material for the $Fe^{3+}/\sum Fe$ reversal attempts was a lherzolite assemblage with about 10% melt, synthesized from MPY30 at 1280° C, 2.5 GPa and $\Delta \log(f_{O_2}) = -2.3$ (WCO). The run product was reground under acetone to grain sizes around 5 μm, and two aliquots were re-equilibrated in olivine capsules with the NNO buffer under H_2O-saturated conditions at 900° C/1 GPa and 1060° C/1 GPa for four and three days, respectively. The reversal run at 900° C was below the solidus and left a previously homogeneous starting spinel zoned with aluminous rims, possibly because of recrystallisation of Al-rich glass inherited from the previous synthesis run. The $K_{D^{Mg-Fe}}^{olv-sp}$ did reset to the lower temperature whereas the $Fe^{3+}/\sum Fe$ ratio in spinel showed little change. The reversal at 1060° C gave largely homogeneous spinels coexisting with olivine and hydrous melt (pyroxenes eliminated). Spinel was reset to the new P/T conditions with respect to $K_{D^{Mg-Fe}}^{olv-sp}$ (lower temperature) and X_{Cr}^{sp} (higher degree of melting in the reversal run). The $Fe^{3+}/\sum Fe$ ratio however, remained unchanged and totals based on a perfect spinel stoichiometry are consistently around 98.5 wt%.

A possible explanation is that oxidation of $Cr-Al$ spinel produces cation deficiencies according to the oxidation reaction $4Fe^{2+}_{(Fe_3O_4)} + O_{2(fluid)} = 4Fe^{3+}_{(\gamma\text{-}Fe_2O_3)} + 2O^{2-}_{(fluid)}$ and vacancies in the octahedral sublattice. To maintain charge balance every third Fe^{3+} ion is expelled from the lattice into the coexisting melt or fluid (Lindsley 1976) and spinel becomes relatively enriched in oxygen. Ferric iron and totals will then come out systematically too low if an ideal $RO:R_2O_3$ (1:1) stoichiometry is assumed.

To test this suggestion, oxygen was analysed directly with the electron microprobe, using a synthetic PC1 crystal calibrated on pure quartz (Table 3). Analytical conditions were 5 kV accelerating voltage and 40 nA beam current, at counting times of 40 sec on both peak and background. The quartz standard was included in each experimental mount to ensure a uniform carbon coating thickness, since carbon is an efficient absorber at low X-ray energies. Relative to the starting spinels (T-2856) the reversal products (T-2931) are distinctly richer in oxygen, with a mean excess (Δ) oxygen (i.e. the difference between oxygen analysed and oxygen expected from stoichiometry) of $+1.6$ wt% absolute (Table 3)[1]. The result implies that the reversal spinels are cation deficient and metastable with respect to the coexisting silicates.

We tentatively conclude that redox equilibria in complex $Cr-Al$ spinels are difficult to reverse within reasonable experimental run times. Sintered oxide mixes and synthesis experiments apparently offer the best chance for achieving redox equilibrium, despite problems in actually demonstrating it. Criteria for equilibrium are homogeneous grains, $Cr/(Cr+Al)$ and $Fe^{3+}/\sum Fe$ ranges in spinel of $\leqq 5$, and $K_{D^{Mg-Fe}}^{olv-sp}$ ranges of $<2\%$ across an experimental charge. Equilibrium will be achieved

[1] Silica in some spinel analyses is due to a slight change in beam alignment when switching voltages from 5 to 15 kV during an analytical routine; it does not contribute toward analysed oxygen. Errors in other elements due to this effect are within the precision of the analyses

Table 3. Oxygen analysis of spinels

Sample No.	$T-2856$ Synthesized spinels			$T-2931$ Reversed spinels					USNM[b] 117075 ± 1 stdev ($n=4$)
SiO_2	0.73	0.59	0.32	0.30	0.15	0.42	0.13	0.58	0.06 ± 0.06
Al_2O3	47.5	46.0	46.8	45.2	40.6	44.4	39.6	38.3	9.9 ± 0.03
Cr_2O_3	22.2	23.4	23.4	23.3	28.7	23.7	29.8	30.1	60.8 ± 0.42
Fe_2O_3	1.21	1.19	0.95	1.45	1.83	1.53	1.71	1.71	3.36 ± 0.11
FeO	7.64	7.86	7.88	8.25	8.76	8.37	9.28	9.14	10.0 ± 0.13
MgO	20.7	20.3	20.6	19.8	19.3	19.6	18.8	18.5	15.3 ± 0.01
Total	99.9	99.4	99.9	98.4	99.4	98.0	99.3	98.3	99.4 ± 0.41
Cations (4 oxygens)									
Al	1.51	1.47	1.48	1.46	1.33	1.45	1.31	1.29	0.37 ± 0.00
Cr	0.47	0.50	0.50	0.51	0.63	0.52	0.66	0.68	1.54 ± 0.00
Fe^{3+}	0.02	0.02	0.02	0.03	0.04	0.03	0.04	0.04	0.08 ± 0.00
Fe^{2+}	0.17	0.18	0.18	0.19	0.20	0.19	0.22	0.22	0.27 ± 0.00
Mg	0.83	0.82	0.82	0.81	0.80	0.81	0.78	0.78	0.73 ± 0.00
Mg#	0.83	0.82	0.82	0.81	0.80	0.81	0.78	0.78	0.73 ± 0.00
Chrome#	0.24	0.25	0.25	0.26	0.32	0.26	0.33	0.34	0.80 ± 0.00
Ferric#	0.12	0.12	0.10	0.14	0.16	0.14	0.14	0.14	0.23 ± 0.01
Oxygen									
Stoich.[a]	40.1	39.6	39.8	39.0	38.5	38.7	38.2	37.8	33.3 ± 0.11
Analysed	40.7	40.5	40.1	40.1	39.6	41.0	40.0	39.6	33.6 ± 0.46
Δ oxygen	+0.6	+0.9	+0.3	+1.1	+1.1	+2.3	+1.8	+1.8	+0.3

[a] Stoichiometric oxygen computed on a silica-free basis assuming perfect $RO:R_2O_3$ (1:1) spinel stoichiometry. [b] Chromite standard USNM 117075 from Jarosewich et al. (1980)

with synthesis experiments, provided run times are sufficiently long and melt is present.

Results

Since all starting compositions are relatively enriched in low-melting compounds, most runs experienced large degrees of melting only a few degrees above their water-saturated solidi. A typical run contains large equant olivine grains, subordinate orthopyroxene, clinopyroxene, euhedral spinel octahedra, and about 10 to 30% interstitial glass with occasional quench pyroxenes, bubbles of a separate fluid phase, in addition to graphite in IW and WCO runs (Fig. 1). Despite relative pyroxene enrichment it proved difficult to keep pyroxenes on the liquidus (and control a_{SiO_2}) especially in olivine capsules. This poses a potential problem for oxygen barometry, since a_{SiO_2} in the melt and a_{mt} in spinel are inversely related through the FMQ equilibrium. If other variables are constant a drop in a_{SiO_2} causes an increase in ferric iron in spinel. However, repetitions of orthopyroxene undersaturated experiments at lower degrees of melting (with orthopyroxene present) did not give different $Fe^{3+}/\sum Fe$ ratios in spinel, suggesting that a_{SiO_2} variations due to excessive melting are small. Experimental spinel, olivine, and orthopyroxene compositions (averages based on at least ten analyses) are given in Table 4.

The redox ratio $Fe^{3+}/\sum Fe$ *in spinel*

The compositional parameter most sensitive of f_{O_2} is the $Fe^{3+}/\sum Fe$ in spinel (c.f. Hill and Roeder 1974). Within the $P-T-X-f_{O_2}$ range covered by our experiments, the ratio exhibits a simple near-linear relationship with $\Delta \log(f_{O_2})$, with a correlation coefficient of 0.98 (Fig. 3). The redox ratio is found to be insensitive to temperature within analytical error (Fig. 4) if spinel is equilibrated along $f_{O_2}-T$ paths parallel to FMQ. A similar $T-f_{O_2}$ relationship was noted for redox equilibria in silicate melts (Carmichael and Ghiorso 1986), implying that the $K_{D Fe^{2+}-Fe^{3+}}^{sp-liq}$ is temperature independent.

The redox ratio in spinel is slightly dependent on pressure. For all starting compositions, $Fe^{3+}/\sum Fe$ in spinel falls with increasing pressure at given $\Delta \log(f_{O_2})$, runs with the WCO buffer being an apparent exception (Fig. 5). This pressure dependence is entirely consistent wit a standard pressure correction based on molar volume changes. Assuming the $K_{D Fe^{2+}-Fe^{3+}}^{sp-liq}$ is pressure independent (or less pressure dependent than the $Fe^{3+}/\sum Fe$ ratio in spinel), then ferric/ferrous iron equilibria in silicate melts can also be expected to fall with increasing pressure at constant $\Delta \log(f_{O_2})$.

Finally, the $Fe^{3+}/\sum Fe$ ratio in spinel is compositionally dependent and falls with increasing $Cr/(Cr+Al)$ ratio at given $\Delta \log(f_{O_2})$ (Fig. 5), suggesting substantial interaction between Cr and Fe^{3+} in the octahedral sublattice. In absolute terms however, both Fe^{2+} and Fe^{3+} in spinel increase with increasing Cr content at given T and $\Delta \log(f_{O_2})$.

The $Cr/\sum R^{3+}$ *ratio in spinel*

The main variables controlling the $Cr/\sum R^{3+}$ ratio in spinel are f_{O_2}, pressure, composition of coexisting phases,

Table 4. Experimental results

Run No	Experimental conditions					Spinel[b]					
	Mix	T °C P	(GPa)	$\Delta \log f_{O_2}$	Time (hours)	Ti	Al	Cr	Fe^{3+}	Fe^{2+}	Mg
						(cations to 4 oxygens)					
1. Fe–FeO experiments (spec-pure iron capsules)											
3041	MPY30	1200	0.5	−3.63	72	0.003	1.449	0.557	0.002	0.370	0.663
3067	S1297	1250	0.4	−3.59	50	0.007	0.500	1.468	0.020	0.537	0.400
2. $WC-WO_2-C$ experiments (graphite capsules)											
2769	MPY30	1050	0.9	−2.36	48	0.001	1.359	0.626	0.013	0.136	0.864
2809	S1297	1050	1.0	−2.37	48	0.001	0.419	1.541	0.037	0.373	0.628
2890	MPY30	1260	1.0	−2.06	12	0.001	1.396	0.583	0.018	0.158	0.844
2833	MPY30	1230	2.2	−2.29	24	0.001	1.395	0.579	0.023	0.127	0.874
2896	MPY30	1100	2.5	−2.56	50	0.010	1.170	0.787	0.024	0.224	0.786
2856	MPY30	1280	2.5	−2.28	22	0.002	1.472	0.504	0.020	0.176	0.826
2839	MPY30	1240	2.7	−2.36	28	0.001	1.327	0.641	0.029	0.167	0.835
3. Ni–NiO experiments (olivine capsules)											
2944	MPY30	1100	0.3	0.79	50	0.002	1.285	0.596	0.114	0.189	0.811
2905	MPY55	1100	1.0	0.57	25	0.008	0.653	1.158	0.173	0.346	0.662
2935	MPY55	1060	1.0	0.57	70	0.007	0.615	1.226	0.144	0.328	0.679
2936	MPY30	1060	1.0	0.57	70	0.003	1.247	0.619	0.128	0.199	0.804
2629	S1297	1300	1.0	0.57	8	0.001	0.201	1.651	0.146	0.276	0.725
2835	S1297	1220	1.0	0.58	12	0.001	0.211	1.677	0.109	0.316	0.685
2926	S1297	1060	2.5	0.09	62	0.002	0.514	1.342	0.140	0.384	0.617
2929	S1297	1080	2.5	0.09	70	0.002	0.364	1.488	0.145	0.383	0.612
2886	MPY30	1100	2.5	0.10	25	0.001	1.407	0.479	0.111	0.204	0.798
2939	S1297	1150	2.5	0.12	48	0.002	0.265	1.607	0.125	0.347	0.640
2883	MPY30	1250	2.5	0.16	8	0.000	1.206	0.715	0.079	0.155	0.846
2887	MPY30	1250	2.5	0.16	8	0.000	1.334	0.592	0.075	0.151	0.849
4. $Fe_3O_4-Fe_2O_3$ experiments (PdAg and olivine capsules)											
2918	MPY30	1050	1.0	5.17	48	0.002	0.956	0.539	0.500	0.124	0.878
2921	S1297	1040	1.0	5.17	72	0.001	0.326	1.143	0.527	0.151	0.851
2933	MPY55	1080	1.0	5.18	68	0.005	0.347	0.977	0.666	0.180	0.825
2795	MPY30	1150	1.0	5.19	12	0.000	0.629	0.548	0.823	0.177	0.823
2853	S1297	1220	1.0	5.20	12	0.001	0.094	1.267	0.638	0.194	0.806
2923	MPY30	1050	2.5	4.29	24	0.001	0.718	0.616	0.664	0.214	0.755
2942	S1297	1150	2.5	4.37	70	0.001	0.300	1.202	0.496	0.175	0.823
2955	MPY30	1150	2.5	4.37	66	0.002	1.137	0.570	0.289	0.097	0.905
2958*	MPY30	1140	2.5	4.37	68	0.002	0.938	0.519	0.539	0.177	0.825
3029*	MPY30	1080	2.5	4.31	72	0.000	0.231	0.483	1.284	0.399	0.602

* 2958: 10 wt% Fe_2O_3, and 3029: 20 wt% Fe_2O_3 added to the starting mix. These runs and the IW experiments are not included in the calibration

[a] Compositional ranges reported as two standard deviations on the ratios $Cr\# = Cr/(Cr+Al)$, $Fe\# = Fe^{3+}/\sum Fe$, $Mg\# = Mg/(Mg+Fe^{2+})$

[b] Silica in all spinel analyses <0.15 wt%

[c] Oxygen fugacities calculated for run temperatures; O'NW = O'Neill and Wall (1987), MW = Mattioli and Wood (1988)

[d] (–) Orthopyroxene undersaturated, n.a. orthopyroxene not analysed

and the degree of fusion. Progressive melting causes a sharp increase in $Cr/\sum R^{3+}$ of residual spinel (c.f. Jaques and Green 1980). Temperature variations at constant degree of melting (variable a_{H_2O}) affect $Cr/\sum R^{3+}$ indirectly through changes in alumina contents in coexisting pyroxene. The effect of pressure at given T and $\Delta \log(f_{O_2})$ within the spinel lherzolite field is to lower $Cr/\sum R^{3+}$ ratios by about 10% (1 to 2.5 GPa), in accordance with previous experimental evidence (Jaques and Green 1980).

For a given bulk composition $Cr/\sum R^{3+}$ of spinel decreases with increasing f_{O_2}, while the $Cr/(Cr+Al)$ ratio rises significantly (c.f. Hill and Roeder 1974). This is a consequence of preferential substitution of Fe^{3+} for Al with increasing availability of ferric iron. ΔG^0 for $Al-Fe^{3+}$ mixing in spinel is significantly larger than for $Cr-Fe^{3+}$; the pseudobinary join $MgAl_2O_4-Fe_3O_4$ is characterized by a wide solvus with a consolute temperature between 900 and 1000° C (Mattioli and Wood 1988), whereas chromite and magnetite appear to be miscible in all proportions down to 600° C (Evans and Frost 1975). Spinels in equilibrium with the MH buffer are comparatively enriched in chromite ($Cr/(Cr+Al)$ up to 0.65) and magnesioferrite components, even in the most aluminous starting mix MPY30.

The degree to which ferric iron can replace Al is limited by the exceptionally high $(Cr+Al)/\sum Fe$ ratios

Tab. 4 (continued)

2 standard deviations[a]			Coexisting phases		$\Delta \log f_{O_2}$ (FMQ)[c]			$FeMg_{-1}$ olv-sp[d]
Cr#	Mg#	Fe#	X_{Mg}^{olv}	X_{Mg}^{opx}	O'NW	MW	This study	This study
0.01	0.01	0.02	0.795	–	−8.44		−7.34	1054
0.04	0.02	0.03	0.765	0.777	−5.95		−4.08	1095
0.04	0.01	0.03	0.940	0.935	−2.90		−2.48	1107
0.04	0.01	0.04	0.903	0.911	−3.35		−1.73	1047
0.02	0.01	0.05	0.921	–	−3.04	−2.49	−2.46	1345
0.03	0.01	0.05	0.936	0.929	−2.74	−0.95	−2.05	1275
0.04	0.01	0.05	0.917	–	−3.46		−2.44	1068
0.02	0.01	0.04	0.904	0.908	−3.71	−2.82	−2.93	1273
0.04	0.01	0.07	0.924	–	−2.85	−1.14	−2.02	1193
0.02	0.02	0.04	0.923	–	0.71	2.78	1.09	1059
0.05	0.02	0.04	0.895	–	−0.39		0.84	1001
0.04	0.02	0.05	0.911	–	−0.44		0.81	1053
0.02	0.01	0.04	0.920	–	0.36	2.55	0.98	1091
0.02	0.02	0.04	0.923	0.919	−0.63		0.91	1293
0.04	0.02	0.02	0.927	–	−1.03		0.62	1124
0.02	0.01	0.02	0.893	0.891	−1.64		0.00	1093
0.02	0.01	0.04	0.913	0.910	−1.27		0.45	1039
0.04	0.02	0.04	0.910	0.908	−0.54	1.66	0.26	1101
0.02	0.01	0.04	0.917	–	−1.58		0.20	1125
0.04	0.01	0.06	0.930	–	−1.10	1.56	−0.23	1288
0.05	0.01	0.06	0.926	0.924	−1.12	1.36	−0.34	1292
0.04	0.01	0.02	0.970	–	4.24	7.85	4.95	1070
0.02	0.01	0.02	0.971	0.948	3.75		4.95	1164
0.02	0.01	0.02	0.966	–	3.84		5.12	1164
0.08	0.01	0.02	0.961	–	4.10		5.27	1174
0.02	0.01	0.04	0.961	–	3.40		4.75	1288
0.10	0.04	0.04	0.956	0.945	2.98		4.60	1053
0.02	0.02	0.04	0.969	0.954	2.96		4.36	1133
0.02	0.01	0.02	0.971	n.a.	2.91	7.09	3.62	1083
0.01	0.01	0.01	0.956	n.a.	2.95	6.43	4.00	1076
0.04	0.01	0.01	0.930	–	2.44		4.72	1181

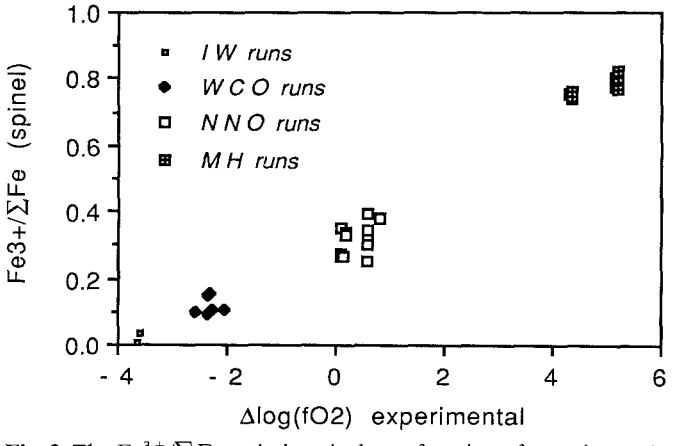

Fig. 3. The $Fe^{3+}/\sum Fe$ ratio in spinel as a function of experimental f_{O_2}. The range in $Fe^{3+}/\sum Fe$ at given $\Delta \log(f_{O_2})$ is due to Cr/Al effects on the ferric/ferrous ratio in spinel (Fig. 5)

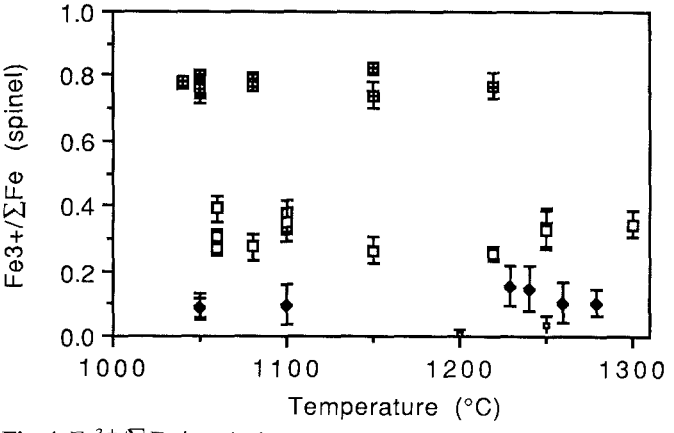

Fig. 4. $Fe^{3+}/\sum Fe$ in spinel versus run temperature; error bars (included where larger than the size of the symbol) are two standard deviations. The redox ratio in spinel is temperature independent within analytical error. Legend as in Fig. 3

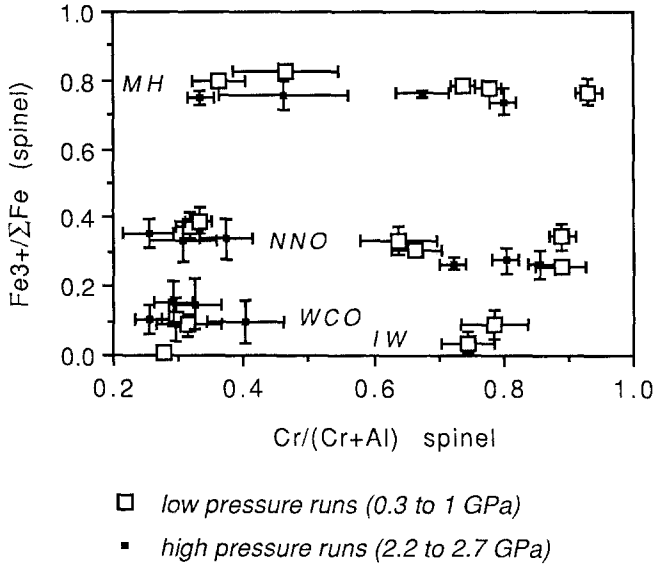

Fig. 5. $Fe^{3+}/\sum Fe$ versus Cr/(Cr + Al) in spinel. Error bars (included where larger than the symbol size) are two standard deviations

(or high modal spinel contents) in the starting compositions. Therefore, two experiments were carried out where the MPY30 starting mix was doped with 10 and 20 wt% hematite (runs 2958 and 3029, Table 4). The maximum Cr/(Cr + Al) ratio in spinel observed is 0.68 (run 3029), despite a low Cr/(Cr + Al) ratio in the starting mix and small degrees of melting. In natural systems where lower normative chromite contents permit greater compositional variability in spinel, oxidized high-temperature spinels are expected to have a high Cr/(Cr + Al) ratio and will be rich in magnetite and magnesioferrite compared with more reduced spinels. Differentiation trends under oxidizing conditions will trend toward ferrite and ulvospinel enrichment without much change in Cr/(Cr + Al) ratio, quite contrary to differentiation trends under low f_{O_2} which lower Cr/(Cr + Al) ratios. The high-temperature magnesioferrite component of oxidized spinels will, however, be quickly eliminated by down-temperature $FeMg_{-1}$ exchange with olivine and pyroxene, and converted to magnetite. Natural examples of high temperature crystallization under oxidizing conditions are Cr-magnetites in Alaskan-type intrusions (Irvine 1967) and the magnesiochromite-ferrite-ulvospinel differentiation series typical of some island arc magmas (Arculus and Wills 1980; see below).

Oxygen barometry

The wide $Cr/\sum R^{3+}$ and $Fe^{3+}/\sum Fe$ ranges covered with our experimental data allow the formulation of an oxygen barometer that is largely based on empirical experimental data. f_{O_2} for the fayalite-ferrosilite-magnetite (FFM) buffer is given by

$$\log f_{O_2}(\mathrm{FFM}) = \Delta S^0/(2.303R) - \Delta H^0/(2.303RT) - P\Delta V/(2.303RT) - 6\log(a_{\mathrm{fa}}^{\mathrm{olv}}) + 3\log(a_{\mathrm{fs}}^{\mathrm{opx}}) + 2\log(a_{\mathrm{mt}}^{\mathrm{spinel}}),$$

and f_{O_2} relative to the FMQ buffer by

$$\Delta\log(f_{O_2})^{\mathrm{FMQ}} = (\Delta S^0_{\mathrm{FFM}} - \Delta S^0_{\mathrm{FMQ}})/(2.303R) - (\Delta H^0_{\mathrm{FFM}} - \Delta H^0_{\mathrm{FMQ}})/(2.303RT) - P(\Delta V_{\mathrm{FFM}} - \Delta V_{\mathrm{FMQ}})/(2.303RT) - 6\log(a_{\mathrm{fa}}^{\mathrm{olv}}) + 3\log(a_{\mathrm{fs}}^{\mathrm{opx}}) + 2\log(a_{\mathrm{mt}}^{\mathrm{spinel}})$$

(where R is the gas constant). A linear least-square fit through the experimental data gives the semi-empirical oxygen geobarometer:

$$\Delta\log(f_{O_2})^{\mathrm{FMQ}} = 0.27 + 2505/T - 400P/T - 6\log(X_{\mathrm{Fe}}^{\mathrm{olv}}) - 3200(1 - X_{\mathrm{Fe}}^{\mathrm{olv}})^2/T + 2\log(X_{\mathrm{Fe}^{2+}}^{\mathrm{sp}}) + 4\log(X_{\mathrm{Fe}^{3+}}^{\mathrm{sp}}) + 2630(X_{\mathrm{Al}}^{\mathrm{sp}})^2/T,$$

where P is in GPa, T in K, $X_{\mathrm{Fe}^{3+}}^{\mathrm{sp}}$ and $X_{\mathrm{Al}}^{\mathrm{sp}}$ the $Fe^{3+}/\sum Fe$ and $Al/\sum R^{3+}$ ratios in spinel, and $X_{\mathrm{Fe}}^{\mathrm{olv}}$ and $X_{\mathrm{Fe}^{2+}}^{\mathrm{sp}}$ the $Fe^{2+}/(Fe^{2+} + Mg)$ ratios in olivine and spinel. To simplify calculations, orthopyroxene is cancelled against the ideal part of $a_{\mathrm{fa}}^{\mathrm{olv}}$. This simplification will introduce a slight systematic error in calculated f_{O_2} because $K_D^{\mathrm{Mg-Fe_{olv-opx}}}$ departs from unity (Sack and Ghiorso 1989), i.e. $6\log(X_{\mathrm{FeM1}}^{\mathrm{opx}} * X_{\mathrm{FeM2}}^{\mathrm{opx}}/X_{\mathrm{Fe}}^{\mathrm{olv}})$ is about -0.25 at an average run temperature of 1150° C and $X_{\mathrm{Fe}}^{\mathrm{olv}} = 0.1$. The $\Delta(\Delta S^0)$ term (0.27) includes a correction for this effect. The pressure dependence of the $Fe^{3+}/\sum Fe$ ratio is calculated with partial molar volume data of Berman (1988), and the $W_{\mathrm{Mg-Fe}}^{\mathrm{olv}}$ interaction term is assumed to be 7000 Jmol^{-1} (Koch-Mueller et al. 1989). Finally, the $\Delta(\Delta H^0)/RT$ term and the regular solution interaction parameter for R^{3+} mixing in spinel are fitted simultaneously with the experimental data.

The above equation is specifically designed for upper mantle-derived rocks. It should not be applied to assemblages significantly more iron-rich than $X_{\mathrm{Fe}}^{\mathrm{olv}} = 0.15$, above which the simplifications regarding orthopyroxene cancellation cannot be expected to be valid. Caution is advised for Cr-rich spinels in the garnet lherzolite and diamond stability fields where nonstoichiometry due to magnesiowüstite or Cr^{2+} substitution in spinel may be a problem, especially at high $X_{\mathrm{Cr}}^{\mathrm{sp}}$ and low f_{O_2} (Ballhaus, unpubl. data; Haggerty 1979). Although orthopyroxene does not apear in the above equation, it is emphasized that calculated $\Delta\log(f_{O_2})$ values are strictly only valid if a_{SiO_2} is buffered by the presence of both olivine and orthopyroxene. However, the barometer gives reasonable results also for orthopyroxene-undersaturated rocks provided calculated f_{O_2} are corrected for that effect. The correction required rarely exceeds -0.2 log units and is approximately three times the shift in a_{SiO_2} relative to orthopyroxene saturation within the a_{SiO_2} range of mantle divided melts (for calculation of a_{SiO_2} from olivine-orthopyroxene equilibria see O'Neill and Wall 1987). a_{SiO_2} estimates for typical melt compositions are given by Ghiorso and Carmichael (1988).

Equilibration temperatures can be calculated with olivine-spinel thermometry (see below), or any other thermometer with proven reliability for mantle assemblages. The choice of the thermometer is not critical in view of the small temperature dependence relative to the FMQ buffer, but a careful evaluation of equilibration temperatures is advisable because of the limited tempera-

ture range of calibration. The fact that our oxygen barometer does not require knowledge of cation ordering in spinel simplifies its use but poses constraints on any application at low temperature where spinels become progressively ordered. Application to natural assemblages suggests that the barometer gives reasonable results down to temperatures around 800° C. It tracks down along $f_{O_2}-T$ paths that are essentially parallel to FMQ and virtually identical to paths obtained with the more complex thermodynamic calibrations (O'Neill and Wall 1987). This does not prove accurate performance at low temperature but does suggest that our empirical model is no less reliable in the low temperature region. The precision within the calibration range (estimated from the standard error of regression) is ± 0.4 log units (above FMQ), and about ± 1.2 to 1.5 log at WCO.

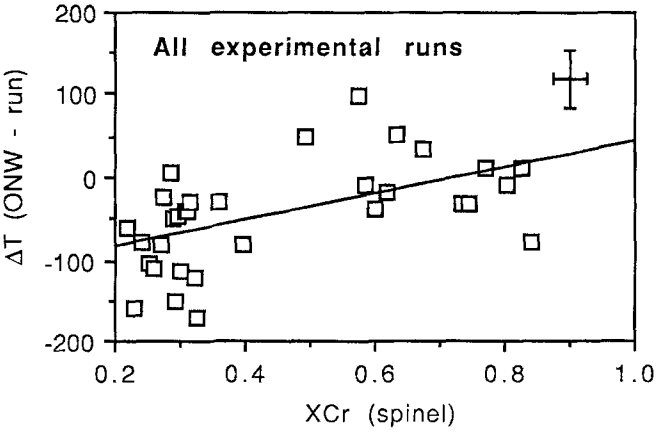

Fig. 6. The difference between calculated $FeMg_{-1}$ exchange (O'Neill and Wall 1987) and experimental temperatures, plotted against the $Cr/(Cr+Al+Fe^{3+})$ ratio in experimental spinels. Linear regression line included for reference. Errors bars illustrate two standard deviations

Olivine-spinel $FeMg_{-1}$ exchange thermometry

Our data provide high precision Mg–Fe olivine-spinel partitioning relations in a compositional and f_{O_2} range where experiments are scarce, and thus offers the opportunity to test and improve existing olivine-spinel $FeMg_{-1}$ exchange thermometers (e.g. Roeder et al. 1979; Fabriès 1979; O'Neill and Wall 1987). The thermometer of O'Neill and Wall gives the closest agreement with run temperatures, although in its present form it tends to underestimate run temperatures progressively with decreasing X^{sp}_{Cr} (Fig. 6). Agreement with experimental temperatures can be significantly improved if ΔG^0 for chromite-ferrite exchange and $Cr-Fe^{3+}$ size mismatch are raised to 9000 and 12000 $Jmol^{-1}$, respectively, and the W^{olv}_{Mg-Fe} parameter to 7000 $Jmol^{-1}$. The corrected and simplified version of the O'Neill-Wall olivine-spinel exchange thermometer then reads:

$$T=(6530+280P+7000+108P)*(1-2X^{olv}_{Fe})-1960$$
$$*(X^{sp}_{Mg}-X^{sp}_{Fe^{2+}})+16150*X^{sp}_{Cr}+25150$$
$$*(X^{sp}_{Fe^{3+}}+X^{sp}_{Ti}))/(R\ln K_D^{Mg-Fe_{olv-sp}}+4.705)$$

where T is in K, X^{sp}_{Ti} the number of Ti cations in spinel to 4 oxygens, K^{olv-sp}_{DMg-Fe} the ratio $(X^{olv}_{Mg}*X^{sp}_{Fe^{2+}})/(X^{olv}_{Fe}*X^{sp}_{Mg})$, and all other notations as above.

The failure of the O'Neill-Wall thermometer to predict accurately the experimental temperatures could point to a systematic error in our calculated $Fe^{3+}/\sum Fe$ ratios (c.f. Wood and Virgo 1989). However, the same systematic relationship is identified when the O'Neill-Wall thermometer is applied to Cr–Al spinels from mantle xenoliths (Fig. 7A). This, and the fact that the improved thermometer version gives temperatures that are virtually independent of X^{sp}_{Cr} (Fig. 7B) strongly suggests that the systematic error suspected in Fig. 6 is inherent in the thermometer of O'Neill and Wall (1987). We conclude that the redox and $FeMg_{-1}$ equilibria in our experiments are internally consistent and accurate.

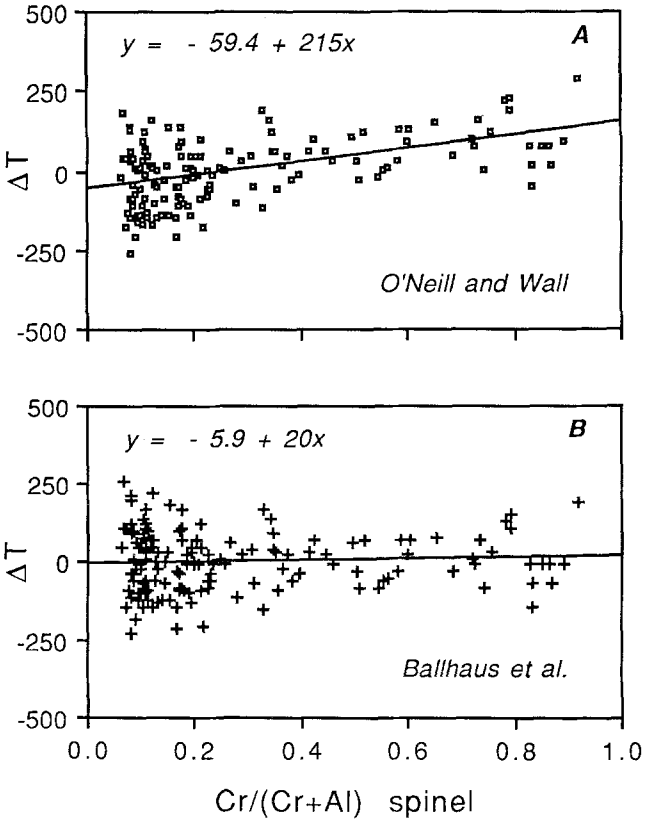

Fig. 7A, B. Comparison between the O'Neill-Wall olivine-spinel thermometer (**A**) and the version suggested in this paper (**B**). ΔT is the deviation of individual calculated $FeMg_{-1}$ temperatures from the mean olivine-spinel temperature of 154 olivine-spinel pairs from spinel lherzolite xenoliths worldwide (c.f. Fig. 10C), plotted against $Cr/(Cr+Al)$ in spinel. Linear regression equations are included in the Figures to quantify systematic errors as a function of $Cr/(Cr+Al)$

Comparison with alternative oxygen barometers

Mattioli and Wood (1988) calibrated magnetite activities along the join $MgAl_2O_4-Fe_3O_4$ between 800 and

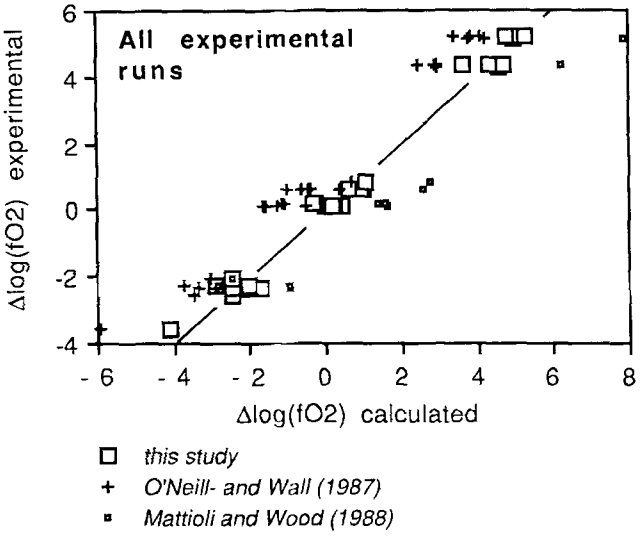

Fig. 8. The olivine-orthopyroxene-spinel oxygen barometer versions of O'Neill and Wall (1987), Mattioli and Wood (1988), and this study applied to the experimental data listed in Table 4. The Mattioli-Wood version is limited by its authors to spinels with $FeCr_2O_4 + FeAl_2O_4 \leqq 30\%$, and only a few experiments meet that requirement

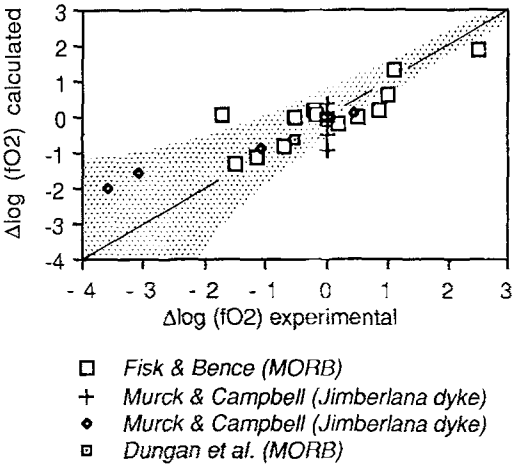

Fig. 9. Calculated versus experimental f_{O_2} for experimental spinel compositions of Dungan et al. (1979), Fisk and Bence (1980), and Murck and Campbell (1986). Where no olivine compositions reported, equilibrium X_{Fe}^{ol} calculated with the olivine-spinel thermometer equation given in this paper; a_{SiO_2} fixed at 0.45 for MORB and 0.38 for the Jimberlana samples, and calculated f_{O_2} values corrected accordingly. Error margins constructed as in Fig. 2. Olivine undersaturated superliquidus runs (e.g. Murck and Campbell 1986) are not plotted because of too large a_{SiO_2} uncertainties

1000° C, by equilibrating synthetic $MgAl_2O_4 - Fe_3O_4$ solid solutions with hematite in a solid-electrolyte cell and measuring the shift in chemical potential of oxygen relative to the MH buffer as a function of X_{mt}^{sp}. The barometer is then derived by fitting a regular solution model to their activity data, assuming a standard cation distribution calculated for 950° C (O'Neill and Navrotsky 1984). The version of O'Neill and Wall (1987), on the other hand, is entirely thermodynamically derived. O'Neill and Wall calculated ideal magnetite activities from the O'Neill-Navrotsky (1984) cation distribution model, with nonideality contributions from size mismatch and reciprocal solution effects. Since all these parameters are calculated simultaneously for each individual spinel analysis, their model is potentially applicable to a wider $T-X$ range than the Mattioli-Wood version.

Mattioli and Wood's (1988) model gives a relatively poor fit to our experimental data. It is too sensitive to small changes in ferric iron contents in spinel in the reduced region (< FMQ − 2) (Fig. 8), and is apparently not applicable to spinels with $Fe^{3+}/\sum Fe$ ratios much lower than 0.15. Above FMQ + 1 it systematically overestimates f_{O_2} by at least two to three log units relative to the experimental conditions. The temperature dependence relative to the FMQ buffer is also larger than supported by our data, and f_{O_2} calculated for a given suite of natural spinels define $f_{O_2} - T$ arrays that are considerably steeper than FMQ (c.f. the "mantle average array" of Mattioli et al. 1989).

The O'Neill-Wall (1987) version gives a slightly better fit. For much of the experimental $T-X-f_{O_2}$ region, agreement between calculated and experimental f_{O_2} is within 1.5 log units, and for the most aluminous spinels at WCO and NNO within 0.5 log units. At MH, however, the model breaks down and underestimates f_{O_2} by about two log units. Correction for $Cr - Fe^{3+}$ size mismatch is too small, and chromites come out up to 1.5 log units lower than Al-spinels at given $\Delta \log(f_{O_2})$. If the excess energies for $Cr - Fe^{3+}$ interaction and chromite-ferrite exchange are raised to the higher values suggested above, the performance of the oxygen sensor significantly improves; systematic errors encountered under strongly oxidizing (MH) conditions, however, remain unaffected by these adjustments.

Application to previous experimental data and natural rocks

In order to test our oxygen barometer we apply it to published synthetic spinel compositions and natural spinels from mantle rocks and mantle-derived melts.

Previous experimental spinel compositions

Dungan et al. (1979), Fisk and Bence (1980), and Murck and Campbell (1986) have crystallized spinel at 10^5 Pa from basaltic melts under controlled f_{O_2}. Unfortunately, for many of their runs olivine compositions are not reported and all runs are orthopyroxene-undersaturated, and thus a_{SiO_2} values are unconstrained. Therefore, equilibrium olivine compositions are estimated by inverting the olivine-spinel thermometer given in this paper and solving for olivine composition at run temperature. a_{SiO_2} values are estimated for the bulk compositions from Ghiorso and Carmichael (1987) and calculated f_{O_2} corrected as described above. The results are shown in Fig. 9.

Agreement between calculated and experimental f_{O_2} is excellent given the uncertainties in olivine composition and a_{SiO_2}. Most runs plot within 0.5 log units of the

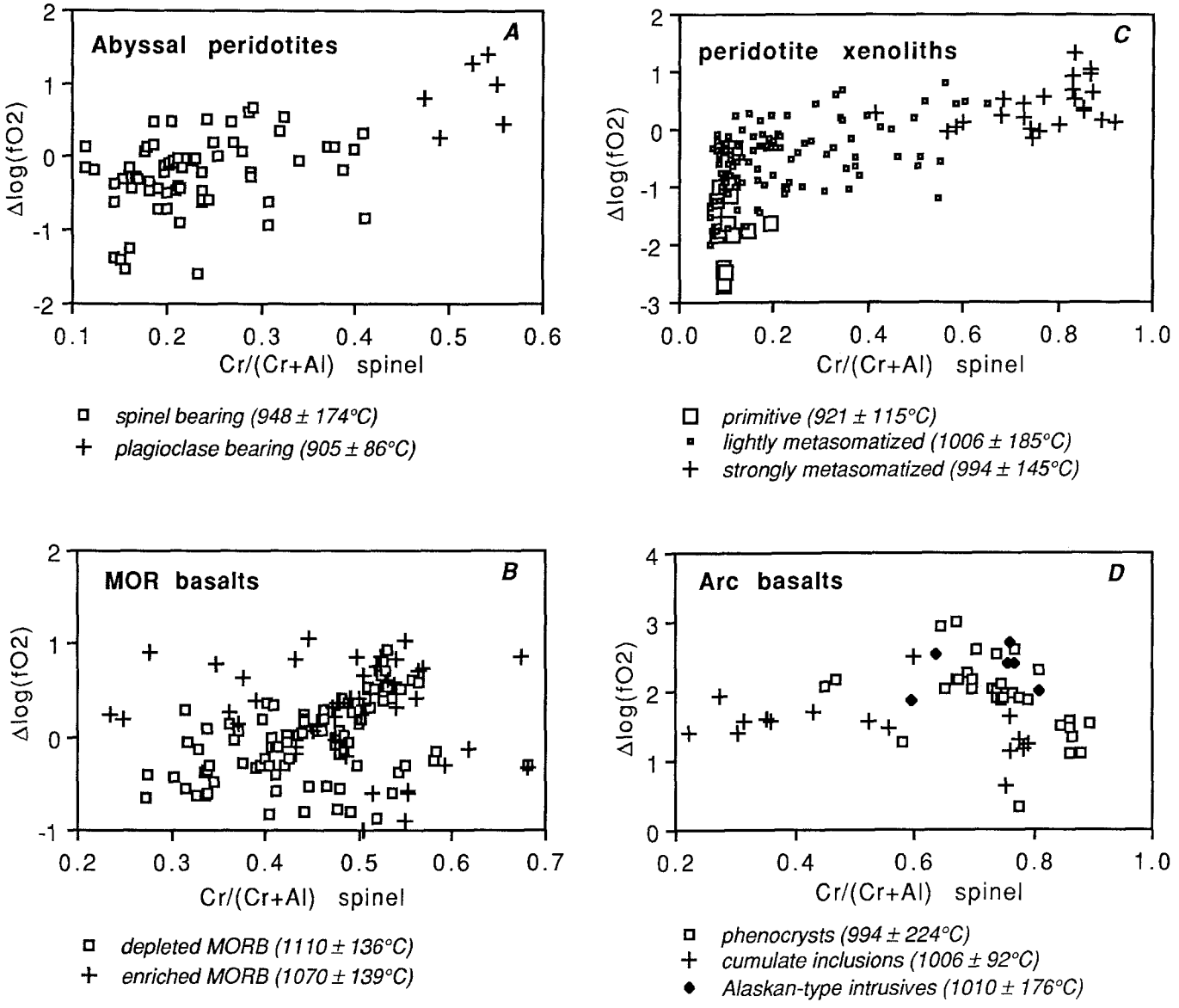

Fig. 10A–D. Application of oxygen barometer (this study) to spinels in mantle rocks and mantle-derived melts. **A** Abyssal spinel and plagioclase peridotites; where no olivine compositions reported (e.g. Dick and Bullen 1984), f_{O_2} calculated for $X_{Fe}^{olv}=0.1$. **B** Mid-ocean ridge basalts (MORB); note the good agreement with abyssal peridotites. **C** Spinel lherzolite and harzburgite xenoliths; note the progressive increase in oxidation state with increasing degree of metasomatism. **D** Spinels in island arc basalts and their cumulate inclusions, and in Alaskan-type intrusions. Average $FeMg_{-1}$ temperatures (this study) with two standard deviations in brackets. $P=1.5$ GPa (spinel peridotites), 0.7 GPa (plagioclase peridotites), and 0.1 GPa (MORB, IAB, and Alaskan-type intrusives). $a_{SiO_2}=0.45$ (MORB) and 0.32 (picritic IAB and Alaskan-type intrusives)

experimental values, and almost all well within the uncertainty ranges that are due to errors in electron microprobe analyses. Three runs only fall significantly off the best-fit line, of which two are in an f_{O_2} region where the errors in calculated $\Delta \log(f_{O_2})$ are at least ± 2 log units.

Application to natural data

Finally, the oxygen barometer is applied to suites of typical mantle rocks and mantle-derived melts (Fig. 10A to D). f_{O_2} values for primitive basalts are calculated using the most magnesian olivine and spinel compositions reported for each suite. Where orthopyroxene is absent a_{SiO_2} values are estimated according to values given by Ghiorso and Carmichael (1987), and calculated f_{O_2} values are corrected as described above.

Abyssal spinel peridotites (Dick and Bullen 1984; Dick 1989) range from mildly reduced (FMQ−2) to moderately oxidized around FMQ (Fig. 10A). Samples above Cr/(Cr+Al) ratios of 0.45 are plagioclase-bearing and might have experienced some oxidation during decompression or alteration. The extensive data set of Dick (1989) does suggests slight regional variations in oxidation state in suboceanic mantle, but f_{O_2} ranges of >5 log units as calculated by Bryndzia et al. (1989) for a similar sample set are clearly exaggerated in view of our

results, and attributed to problems with the Mattioli-Wood oxygen barometer.

Calculated f_{O_2} values for MORB (Ayuso et al. 1976; Sigurdsson 1977; Sigurdsson and Schilling 1976; Dungan et al. 1979; Bryan et al. 1981; Dick and Bryan 1978; Furuta and Tokuyama 1983; Natland et al. 1983; Thy 1983; Batiza and Vanko 1984; Neumann and Schilling 1984; Davis and Clague 1987; Natland 1989) show good agreement with abyssal peridotites, the presumed residues from MORB (Fig. 10B). The results agree well with oxidation states calculated from whole-rock ferric/ferrous iron ratios (Christie et al. 1986). It is interesting to note that spinels from enriched MORB are statistically more oxidized than spinels from depleted MORB, suggesting that the enriched component (le Roex 1987) is oxided relative to primitive oceanic lithosphere (i.e. FMQ and higher). The most aluminous MORB spinels, i.e. those usually regarded as high pressure megacrysts (Sigurdsson and Schilling 1976; Green et al. 1979; Fisk and Bence 1980), give f_{O_2} values that are up to one log unit lower than coexisting low pressure magnesiochromites. The interpretation of these spinels as high pressure phenocrysts would carry the connotation of progressively lower f_{O_2} with depth, and oxidation during ascent by H_2-CH_4 degassing or decompression.

An interesting relationship is evident between calculated f_{O_2} and the degree of fertility of spinel lherzolite nodules (Fig. 10C). Fertile, unmetasomatized lherzolitic mantle samples (Kyser et al. 1981; Preß et al. 1986) apparently are moderately reduced, perhaps recording oxidation states typical of undepleted continental lithosphere. The large group of slightly metasomatized spinel lherzolites and harzburgites with variable degrees of LREE and LIL enrichment and occasional pargasitic amphibole (Sachleben und Seck 1980; Kurat et al. 1980; Fujii and Scarfe 1982; Brearley et al. 1984; Della Giusta et al.. 1986. Furnes et al. 1986; Gutmann 1986; Francis 1987; Canil et al. 1990) is more oxidized and defines an oxidation trend toward FMQ. Extensively metasomatized samples with Ti- and Mn-enriched chromites, abundant phlogopite and K-richterite (Reid et al. 1975; Jones et al. 1983; Dawson and Smith 1988; Winterburn et al. 1990) give oxidation states well above FMQ. It is apparent that the metaxomatizing agents (e.g. Green and Wallace 1988) are oxidizing relative to primitive lithosphere.

Spinels from primitive island arc basalts and cumulate nodules therein (Irvine 1973; Arculus 1978; Tatsumi and Ishizaka 1982; Conrad and Kay 1984; Ramsay et al. 1984; Johnson et al. 1985; DeBari et al. 1987; Dick and Bullen 1984; Nye and Reid 1986; Nye and Turner 1990; Barsdell and Berry 1990; S. Eggins, unpubl. data from Vanuatu) as well as Alaskan-type intrusives (Irvine 1967) are systematically enriched in magnesiochromite and magnetite components relative to MORB, and are highly oxidized (Fig. 10D). f_{O_2} values are calculated for an a_{SiO_2} fixed at 0.32, appreciating the fact that the melts parental to these spinels are mostly nepheline-normative pricrites and ankaramites. Even at such low a_{SiO_2} most island arc spinels plot significantly above the NNO buffer, supporting conclusions reached previously that oxidation states in arc lavas are high (Arculus and Wills 1980; Arculus 1985).

Concluding remarks

Application of our oxygen barometer to typical mantle rocks and mantle-derived primitive melts reveals the following trends. Undepleted, fertile mantle regions and their partial melts are moderately reduced (around FMQ−2). Depleted mid-ocean ridge basalts (MORB) and abyssal peridotites plot around FMQ−1, possibly characterizing typical f_{O_2} conditions of the uppermost oceanic lithosphere. "Enriched" MORB and metasomatized spinel harzburgites are systematically more oxidized between FMQ and FMQ+1. Spinels from island arc basalts and Alaskan-type intrusives are the most oxidized and plot consistently around FMQ+2.

Our results have important implications for the understanding of mantle processes: (1) Mantle metasomatism appears to be coupled with oxidation. If f_{O_2} values calculated for the most metasomatized samples are taken as a reasonable lower limit, then the enriched component may be as oxidized as FMQ+1 to FMQ+2. (2) If f_{O_2} conditions calculated for arc magmas (FMQ+2) represent oxidation states in the mantle sources, then sulphides may be unstable beneath volanic arcs (c.f. Carroll and Rutherford 1987) and chalcophile elements will behave incompatibly during partial melting. It follows that primitive island arc magmas can be expected to be enriched in chalcophile elements, and it is certainly no coincidence that Alaskan-type ultramafic intrusives (Barron et al. 1990; Nixon et al. 1989), the subvolcanic equivalents of arc picrites and ankaramites, often host significant platinum-group element deposits. Reduced carbon is similarly unstable but carbonate or carbonatitic melts may occur. (3) Recycling of relatively oxidized lithosphere at convergent plate boundaries may cause secular variations in oxidation state (Arculus 1985) and may be the major control for the large-scale f_{O_2} structure of the Earth's mantle (c.f. Haggerty 1986; Green et al. 1987; Ballhaus et al. 1990). In this context, the low oxidation states in diamond-bearing lithosphere may be interpreted as a relict from earlier stages of the Earth's history when conditions in the Upper mantle were generally more reduced (Arculus 1985), with diamonds forming where oxidized recycled material (CO_2-rich silicate or carbonatitic melts; Wallace and Green 1988) interacts with reduced (IW) lithosphere (in contrast to Kesson and Ringwood 1989). Alternatively, the presence of diamonds may be indicative of lithosphere reduction by continuing outgassing of reduced CH_4-H_2 fluids from deeper mantle, as suggested by Green et al. (1987) and Taylor and Green (1988).

Acknowledgments. We thank S.Y. O'Reilly, R.J. Arculus, R.A. Binns, S.M. Eggins, and S.S. Sun for critical reviews which greatly improved the final version. Keith Harris, Simon Stevens, and Wieslav Jablonski provided valuable technical assistance. Steve Eggins kindly made available unpublished spinel analyses from Vanuatu. R.A. Binns is thanked for efficient editorial handling of the manuscript. We also appreciate some comments of H.St.C. O'Neill on an earlier version of this paper. CB wishes to thank Professor D. Jung, University of Hamburg, for his support during the past three years. Generous financial support was provided by a DFG grant to CB and an ARC grant to DHG.

References

Arculus RJ (1978) Mineralogy and petrology of Grenada, Lesser Antilles Island Arc. Contrib Mineral Petrol 65:413–424

Arculus RJ (1985) Oxidation status of the mantle: past and present. Ann Rev Earth Planet Sci 13:75–95

Arculus RJ, Wills KJA (1980) The petrology of plutonic blocks and inclusions from the Lesser Antilles island arc. J Petrol 21:743–799

Ayuso RA, Bence AE, Taylor SR (1976) Upper Jurassic tholeiitic basalts from DSDP Leg 11. J Geophys Res 81:4305–4325

Ballhaus C, Berry RF, Green DH (1990) Oxygen fugacity controls in the Earth's upper mantle. Nature 349:437–440

Barron LM, Slansky E, Suppel D, Johan Z, Ohnenstetter M (1990) Late- to post-magmatic PGE mineralisation in the Fifield platinum province and the Owendale Intrusive Complex, NSW (abstract). 10th Australian Geological Congress, Geol Soc Austr, pp 132

Barsdell M, Berry RF (1990) Origin and evolution of primitive island arc ankaramites from Western Epi, Vanuatu. J Petrol 31:747–777

Batiza R, Vanko D (1984) Petrology of young Pacific seamounts. J Geophys Res 89:11235–11260

Berman RG (1988) Internally-consistent thermodynamic data for minerals in the system $K_2O-Na_2O-CaO-MgO-FeO-Fe_2O_3-Al_2O_3-SiO_2-TiO_2-H_2O-CO_2$. J Petrol 29: 445–522

Brearley M, Scarfe CM, Fujii T (1984) The petrology of ultramafic xenoliths from Summit Lake, near Prince George, British Columbia. Contrib Mineral Petrol 88:53–63

Bryan WB, Thompson G, Ludden JN (1981) Compositional variation in normal MORB from 22°–25°N: Mid-Atlantic ridge and Kane fracture zone. J Geophys Res 86:11815–11836

Bryndzia LT, Wood BJ, Dick HJB (1989) The oxidation state of the Earth's sub-oceanic mantle from oxygen thermobarometry of abyssal peridotites. Nature 341:526–527

Canil D, Virgo D, Scarfe CM (1990) Oxidation state of mantle xenoliths from British Columbia, Canada. Contrib Mineral Petrol 104:453–462

Carmichael ISE, Ghiorso MS (1986) Oxidation-reduction relations in basic magmas: a case for homogeneous equilibria. Earth Planet Sci Lett 78:200–210

Carroll MR, Rutherford MJ (1987) The stability of igneous anhydrite: experimental results and implications for sulfur behavior in the 1982 El Chichon trachyandesite and other evolved magmas. J Petrol 28:781–801

Christie DM, Carmichael ISE, Langmuir CH (1986) Oxidation states of mid-ocean ridge basalt glasses. Earth Planet Sci Lett 79:397–411

Conrad WK, Kay RW (1984) Ultramafic and mafic inclusions from Adak Island: crystallization history, and implications for the nature of primary magmas and crustal evolution in the Aleutian arc. J Petrol 25:88–125

Davis AS, Clague DA (1987) Geochemistry, mineralogy, and petrogenesis of basalt from the Gorda Ridge. J Geophys Res 92:10467–10483

Dawson JB, Smith JV (1988) Metasomatized and veined upper-mantle xenoliths from Pello Hill, Tanzania: Evidence for anomalously-light mantle beneath the Tanzanian sector of the East African Rift Valley. Contrib Mineral Petrol 100:510–527

Della Giusta A, Princivalle F, Carbonin S (1986) Crystal chemistry of natural Cr-bearing spinels with $0.15 \leqq Cr \leqq 1.07$. Neues Jahrb Mineral Abh 155:319–330

DeBari S, Kay SM, Kay RW (1987) Ultramafic xenoliths from Adagdak volcano, Adak, Aleutian island, Alaska: deformed igneous cumulates from the MOHO of an island arc. J Geol 95:329–341

Dick HJB (1989) Abyssal peridotites, very slow spreading ridges and oceanic ridge magmatism. In: Saunders AD, Norry MJ (eds) Magmatism in oceanic basins. Geol Soc Spec Publ 42, Blackwell, Oxford, pp 71–105

Dick HJB, Bryan WB (1978) Variation of basalt phenocryst mineralogy and rock compositions in DSDP hole 396B. Init Rep DSDP 46:215–224

Dick HJB, Bullen T (1984) Chromian spinel as petrogenetic indicator in abyssal and alpine-type periodotites and spatially associated lavas. Contrib Mineral Petrol 86:54–76

Dungan MA, Long PE, Rhodes JM (1979) The petrography, mineral chemistry, and one-atmosphere phase relations of basalts from site 395. Init Rep DSDP 45:461–472

Dyar MD, McGuire AV, Ziegler RD (1989) Redox equilibria and crystal chemistry of coexisting minerals from spinel lherzolite mantle xenoliths. Am Mineral 74:969–980

Eggler DH (1983) Upper mantle oxidation state: evidence from olivine-orthopyroxene-ilmenite assemblages. Geophys Res Lett 10:365–368

Evans BW, Frost BR (1975) Chrome-spinel in progressive metamorphism – a preliminary analysis. Geochim Cosmochim Acta 39:959–972

Fabriès J (1979) Spinel-olivine geothermometry in peridotites from ultramafic complexes. Contrib Mineral Petrol 69:329–336

Falloon TJ, Green DH (1987) Anhydrous partial melting of MORB pyrolite and other periodotite compositions at 10 kb: implications for the origin of primitive MORB glasses. Mineral Petrol 37:181–219

Fisk MR, Bence AE (1980) Experimental crystallization of chrome spinel in FAMOUS basalt 527–1–1. Earth Planet Sci Lett 48:111–123

Francis D (1987) Mantle-melt interaction recorded in spinel lherzolite xenoliths from the Alligator Lake volcanic complex, Yukon, Canada. J Petrol 28:569–597

Fujii T, Scarfe CM (1982) Petrology of ultramafic nodules from West Kettle River, near Kelowna, sourthern British Columbia. Contrib Mineral Petrol 80:297–306

Furnes H, Pedersen RB, Maaløe S (1986) Petrology and geochemistry of spinel peridotite nodules and host basalt, Vestspitsbergen. Nor Geol Tiddskr 66:53–68

Furuta T, Tokuyama H (1983) Chromian spinels in Costa Rica basalts, Deep Sea Drilling Project site 505 – a preliminary interpretation of electron microprobe analyses. Init Repts DSDP 69:805–811

Ghiorso MS, Carmichael ISE (1988) Modelling magmatic systems: petrologic applications. In: Carmichael, ISE, Eugster HP (eds) Thermodynamic modelling of geological materials: Minerals, fluids and melts. Reviews in Mineralogy, vol 17. Mineral Soc Am, pp 467–499

Green DH, Ringwood AE (1967) The genesis of basaltic magmas. Contrib Mineral Petrol 15:103–190

Green DH, Wallace ME (1988) Mantle metasomatism by ephemeral carbonatite melts. Nature 336:459–462

Green DH, Hibberson WO, Jaques AL (1979) Petrogenesis of mid-ocean ridge basalts. In: McElhinney MW (ed) The earth: Its origin, structure, and evolution. Acad Press, London, pp 265–299

Green DH, Falloon TJ, Taylor WR (1987) Mantle-derived magmas – roles of variable source peridotite and variable C–H–O fluid compositions. In: Mysen BO (ed) Magmatic processes. Physicochemical principles. Geochem Soc, London, pp 139–154

Grove TL (1981) Use of FePt alloys to eliminate the iron loss problem in 1 atmosphere gas mixing experiments: theoretical and practical considerations. Contrib Mineral Petrol 78:298–304

Gutmann JT (1986) Origin of four- and five-phase ultramafic xenoliths from Sonora, Mexico. Am Mineral 71:1076–1084

Haggerty SE (1979) Spinels in high pressure regimes. In: Boyd FR, Meyer HOA (eds) The mantle sample:Inclusions in kimberlites and other volcanics. 2nd Intern. Kimberlite Conf Santa Fe, pp 183–196

Haggerty SE (1986) Diamond genesis in a multiply-constrained model. Nature 320:34–39

Hill RET, Roeder PL (1974) The crystallization of spinel from basaltic liquid as a function of oxygen fugacity. J Geol 82:709–729

Huebner JS (1971) Buffering techniques for hydrostatic systems at elevated pressures. In: Ulmer GC (ed) Research techniques

for high pressure and high temperatures. Springer, Berlin Heidelberg New York, pp 123–177
Irvine TN (1967) Chromian spinel as petrogenetic indicator. Part. 2. Petrologic applications. Can J Earth Sci 4:71–103
Irvine TN (1973) Bridget Cove volcanics, Juneau Area, Alaska: Possible parental magma of Alaskan-type ultramafic complexes. Carnegie Inst Washington Yearb 72:478–491
Jaques AL, Green DH (1980) Anhydrous melting of peridotite at 0–15 kbar pressure and the genesis of tholeiitic basalts. Contrib Mineral Petrol 73:287–310
Jarosewich E, Nelen JA, Norberg JA (1980) Reference samples for electron microprobe analysis. Geostand Newslett 4:43–47
Johnson RW, Jaques AL, Hickey RL, McKee CO, Chappell BW (1985) Manam Island, Papua New Guinea: Petrology and geochemistry of a low-TiO_2 basaltic island-arc volcano. J Petrol 26:283–323
Jones AP, Smith JV, Dawson JB (1983) Glasses in mantle xenoliths from Olmani, Tanzania. J Geol 91:167–178
Kesson SE, Ringwood AE (1989) Slab-mantle interactions 2. The formation of diamonds. Chem Geol 78:97–118
Koch-Mueller M, Cemic L, Langer K (1989) An experimental study of orthopyroxene = olivine + quartz equilibria (Abstr.). Terra Abstracts 1:140
Kurat G, Palme H, Spettel B, Baddenhausen H, Hofmeister H, Palme C, Wänke H (1980) Geochemistry of ultramafic xenoliths from Kapfenstein, Austria: evidence from a variety of upper mantle processes. Geochim Cosmochim Acta 44:45–60
Kyser TK, O'Neil JR, Carmichael ISE (1981) Oxygen isotope thermometry of basic lavas and mantle nodules. Contrib Mineral Petrol 77:11–23
le Roex AP (1987) Source regions of mid-ocean ridge basalts: evidence for enrichment processes. In: Menzies MA, Hawkesworth CJ (eds) Mantle metasomatism. Acad Press London, pp 389–421
Lindsley DH (1976) The crystal chemistry and structure of oxide minerals as exemplified by the Fe–Ti oxides. In: Rumble III D (ed) Oxide Minerals. Reviews in Mineralogy, vol 3. Miner Soc Am, pp L1–L60
Lucas H, Muggeridge MT, McConchie DM (1988) Iron in kimberlitic ilmenites and chromian spinels: a survey of analytical techniques. In: Ross J (ed) Kimberlites and related rocks: 4th Intern Kimberlite Conf Perth, pp 311–320
Mattioli GS, Wood BJ (1988) Magnetite activities across the $MgAl_2O_4-Fe_3O_4$ spinel join, with application to thermobarometric estimates of upper mantle oxygen fugacity. Contrib Mineral Petrol 98:148–162
Mattioli GS, Baker MB, Rutter MJ, Stolper EM (1989) Upper mantle oxygen fugacity and its relationship to metasomatism. J Geol 97:521–536
McGuire AV, Dyar MD, Ward KA (1989) Neglected Fe^{3+}/Fe^{2+} ratios: a study of Fe^{3+} content of megacrysts from alkali basalts. Geology 17:687–690
Murck BW, Campbell IH (1986) The effects of temperature, oxygen fugacity and melt composition on the behaviour of chromium in basic and ultrabasic melts. Geochim Cosmochim Acta 50:1871–1887
Natland JH (1989) Partial melting of a lithologically heterogeneous mantle: inferences from crystallization histories of magnesian abyssal tholeiites from the Siqueiros Facture Zone. In: Saunders AD, Norry MJ (eds) Magmatism in the ocean basins. Geol Soc Spec Publ 42, Blackwell, Oxford, pp 41–70
Natland JH, Adamson AC, Laverne C, Melson WG, O'Hearn T (1983) A compositionally nearly steady-state magma chamber at the Costa Rica rift: evidence from basalt glass and mineral data. Init Rep DSDP 69:811–858
Neumann ER, Schilling JG (1984) Petrology of basalts from the Mohns-Knipovich ridge; the Norwegian-Greenland sea. Contrib Mineral Petrol 85:209–223
Nixon GT, Cabri LJ, Laflamme JHG (1989) Provenance of platinum nuggets in Tulameen placer deposits (abstract). Bull Geol Soc Finl 61 (5th Intern Platinum Conf): 45
Nye CJ, Reid MR (1986) Geochemistry of primary and least fractionated lavas from Okmok volcano, central Aleutians: implications for arc magmagenesis. J Geophys Res 91:10271–10287
Nye CJ, Turner DL (1990) Petrology, geochemistry, and age of the Spurr volcanic complex, eastern Aleutian arc. Bull Volcanol 52:205–226
O'Neill HStC (1987a) The quartz-fayalite-iron and quartz-fayalite-magnetite equilibria and the free energies of formation of fayalite (Fe_2SiO_4) and magnetite (Fe_3O_4). Am Mineral 72:67–75
O'Neill HStC (1987b) The free energies of formation of NiO, CoO, Ni_2SiO_4. Am Mineral 72:280–291
O'Neill HStC, Navrotsky A (1984) Cation distributions and thermodynamic properties of binary spinel solid solutions. Am Mineral 69:733–753
O'Neill HStC, Wall VJ (1987) The olivine-orthopyroxene-spinel oxygen geobarometer, the nickel precipitation curve, and the oxygen fugacity of the Earth's upper mantle. J Petrol 28:1169–1191
Preß S, Witt G, Seck HA, Eonov D, Kovalenko VL (1986) Spinel peridotite xenoliths from the Tariat depression, Mongolia. I: Major element chemistry and mineralogy of a primitive mantle xenolith suite. Geochim Cosmochim Acta 50:2587–2599
Ramsay WRH, Crawford AJ, Foden JD (1984) Field setting, mineralogy, chemistry and genesis of arc picrites, New Georgia, Solomon Islands. Contrib Mineral Petrol 88:386–402
Reid AM, Donaldson CH, Brown RW, Ridley WI, Dawson JB (1975) Mineral chemistry of peridotite xenoliths from the Lashaine volcano, Tanzania. Phys Chem Earth 9:525–543
Roeder PL, Campbell IH, Jamieson H (1979) A re-evaluation of the olivine-spinel geothermometer. Contrib Mineral Petrol 68:325–334
Sachtleben T, Seck HA (1980) Chemical control on Al solubility in orthopyroxene, and its implications on pyroxene geothermometry. Contrib Mineral Petrol 78:157–165
Sack RO, Ghiorso MS (1989) Importance of considerations of mixing properties in establishing an internally consistent thermodynamic database: thermochemistry of minerals in the system $Mg_2SiO_4-Fe_2SiO_4-SiO_2$. Contrib Mineral Petrol 102:41–68
Schwab RG, Küstner D (1981) Die Gleichgewichtsfugazitäten technologisch und petrologisch wichtiger Sauerstoffpuffer. Neues Jahrb Mineral Abh 140:111–142
Sigurdsson H (1977) Spinels in Leg 37 basalts and peridotites: phase chemistry and zoning. Init Rep DSDP 37:883–891
Sigurdsson H, Schilling JG (1976) Spinels in mid-Atlantic ridge basalts: chemistry and occurrence. Earth Planet Sci Lett 29:7–20
Tatsumi Y, Ishizaka K (1982) Magnesian andesite and basalt from Shodo-shima island, southwest Japan, and their bearing on the genesis of calc-alkaline andesites. Lithos 15:161–172
Taylor WR, Foley SF (1989) Improved oxygen-buffering techniques for C–O–H fluid-saturated experiments at high pressure. J Geophys Res 94:4146–4158
Taylor WR, Green DH (1987) Measurement of reduced peridotite-C–O–H solidus and implications for redox melting of the mantle. Nature 332:349–352
Thy P (1983) Spinel minerals in transitional and alkali basaltic glasses from Iceland. Contrib Mineral Petrol 83:141–149
Wallace ME, Green DH (1988) An experimental determination of primary carbonatite magma compostion. Nature 335:343–346
Winterburn PA, Harte B, Gurney JJ (1990) Peridotite xenoliths from the Jagersfontein kimberlite pipe: I. Primary and primary-metasomatic mineralogy. Geochim Cosmochim Acta 54:329–341
Wood BJ, Virgo D (1989) Upper mantle oxidation state: ferric iron contents of lherzolite spinels by ^{57}Fe Mössbauer spectroscopy and resultant oxygen fugacities. Geochim Cosmochim Acta 53:1277–1291

Editorial responsibility: R. Binns